AIAA JOURNAL
Vol. 44, No. 1, January 2006

Plasma Actuators for Separation Control of Low-Pressure Turbine Blades

Junhui Huang,* Thomas C. Corke,† and Flint O. Thomas‡
University of Notre Dame, Notre Dame, Indiana 46556

This work involves the documentation and control of flow separation that occurs over turbine blades in the low-pressure-turbine (LPT) stage at the low Reynolds numbers typical of high-altitude cruise. We utilize a specially constructed linear cascade that is designed to study the flowfield over a generic LPT cascade consisting of Pratt and Whitney "Pak B" shaped blades. The center blade in the cascade is instrumented to measure the surface-pressure coefficient distribution. Optical access allows laser-Doppler-velocimetry measurements for boundary-layer profiles. Experimental conditions were chosen to give a range of chord Reynolds numbers from 10^4 to 10^5, and a range of freestream turbulence levels from $u'/U_\infty = 0.08$ to 2.85%. The surface-pressure measurements were used to define a region of separation and reattachment that depends on the freestream conditions. The location of separation was found to be relatively insensitive to the experimental conditions. However, the reattachment location was very sensitive to the turbulence level and Reynolds number. In the absence of separation, excellent agreement was found between the measured pressure distributions and predictions from Euler simulations. Separation control was performed using a single-dielectric-barrier-discharge plasma actuator that is placed at different chord locations, upstream of the separation line. The actuator is designed to produce a steady two-dimensional jet, which is locally parallel to the blade surface. This is intended to add momentum to the near-wall boundary layer. Reattachment occurred in all cases. The amplitude level of the actuator was varied to determine its effect on the reattachment location.

Nomenclature

C	=	axial chord length
C_p	=	pressure coefficient
$\boldsymbol{E}$	=	electric field vector
e	=	elementary charge
$\boldsymbol{F}_B$	=	body force generated by plasma
k	=	Boltzmann constant
n_0	=	plasma density
P_s	=	static pressure
P_∞	=	static pressure in the freestream
q	=	dynamic pressure
Re_c	=	Reynolds number based on axial chord length and freestream velocity
T_i, T_e	=	ion and electron temperatures
U_∞	=	freestream velocity
u, v, w	=	velocity components
u', v', w'	=	rms velocities
x, y	=	axial coordinates
ϵ_0	=	permittivity of free space
λ_D	=	Debye length
ρ	=	density of air
ϕ	=	electric potential

I. Introduction

EXPERIMENTAL results from jet-engine tests have indicated that the unsteady blade-row interactions and suction-side separation can have a significant impact on the efficiency of turbine stages. These effects can become further exacerbated in the low-pressure-turbine (LPT) stages because of the combination of high temperature and low density. A map of the Reynolds numbers at different locations in a turbine engine (PW2037) by Hourmouziadis[1] showed order-of-magnitude lower values (of the $\mathcal{O}$100,000) in the LPT compared to other locations. During high-altitude cruise, the chord Reynolds number of the LPT blades can drop below 2.5×10^4. Sharma[2] indicated a nearly 300% rise in the loss coefficient when the Reynolds number falls below 2×10^5. He found this to be primarily associated with a laminar separation over the trailing half of the blade suction surface.

At such low Reynolds numbers, the boundary layers on the LPT blades are largely laminar. As a result, their development is extremely sensitive to unsteady disturbances. For example, Sharma[2] found that the size of the separation bubble and location of turbulence transition were significantly impacted by the turbulence levels and other freestream unsteadiness.

Although passive measures for avoiding laminar separation might be advisable, such standard methods as altering the blade shape, or using boundary-layer trips or vortex generators can produce a detrimental effect on the engine performance when higher Reynolds numbers exist at lower altitudes. In addition, from an engine design standpoint a lower number of more highly loaded stages, with a greater potential for flow separation, are desirable to minimize engine cost, weight, and length. Therefore on-demand active separation control provides the best opportunity to achieve an overall improvement in engine performance and will likely lead to enhanced designs with a lower part count, size, and weight.

The potential this offers has motivated work on controlling flow separation over LPT blades. Lake et al.[3] and Bons et al.[4] used a linear cascade of Pak B blades to simulate the pressure gradient for a generic LPT blade row. Lake et al. applied spherical dimples into the surface of the blades to passively force flow reattachment. Bons et al. used steady blowing of air through angled holes in the blade surface. Both approaches aimed to produce streamwise vortices like those used to prevent flow separation on aircraft wings and in diffusers.

Our approach for separation control on the LPT blades is based on the use of single-dielectric-barrier-discharge (SDBD) plasma actuators. These actuators consist of electrodes that are located on the surface of the blades. A high-voltage ac supplied to the electrodes

Presented as Paper 2003-1027 at the Aerospace Sciences Conference, Reno, NV, 2 January 2003; received 5 June 2003; revision received 10 April 2004; accepted for publication 22 January 2005.

*Graduate Assistant, Center for Flow Physics and Control, Aerospace and Mechanical Engineering Department.

†Clark Chair Professor, Center for Flow Physics and Control, Aerospace and Mechanical Engineering Department. Associate Fellow AIAA.

‡Professor, Center for Flow Physics and Control, Aerospace and Mechanical Engineering Department. Associate Fellow AIAA.

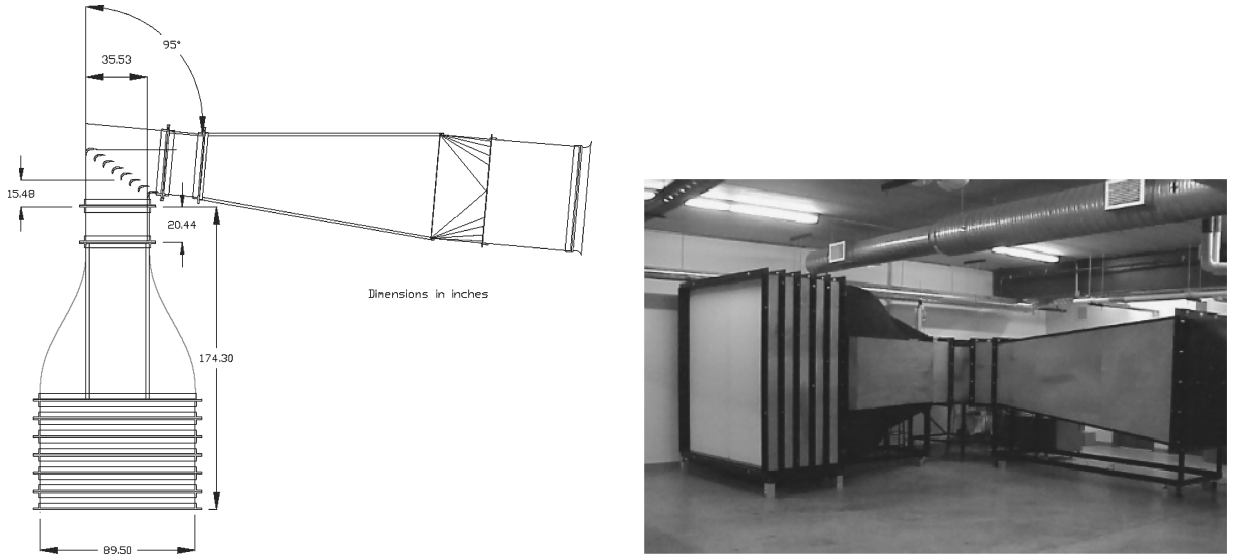

Fig. 1 Schematic and photograph of the linear cascade facility (schematic dimensions in inches).

causes the air in their vicinity to weakly ionize. The ionized air (plasma) in the presence of the electric field gradient produced by the electrodes results in a body force vector acting on the external flow that can induce steady or unsteady velocity components. Numerical simulations[5] of the electric field, body force, and induced velocities have led to optimized designs. Descriptions of our actuator designs are presented by Corke and Matlis[6] and Post.[7] Examples of different applications include exciting boundary-layer instabilities on a sharp cone at Mach 3.5 by Corke et al.[8]; lift augmentation on a wing section by Corke et al.[9]; and wing-section leading-edge separation control by Post and Corke.[10] Other recent experiments that utilized plasma actuators for separation control in turbine-blade simulations are Hultgren and Ashpis[11] and List et al.[12]

II. Experimental Setup

A specially designed linear cascade wind tunnel was built for the experiments. A schematic of the tunnel is shown in Fig. 1. The freestream turbulence level upstream of the cascade was $u'/U_\infty = 0.08\%$. This included all frequencies in a band from 1 Hz to 5 kHz.

A straight section following the contraction gives access to place turbulence generating devices upstream of the cascade. The inlet to the cascade has a 35.5-in. (0.9-m) square cross-section dimension. The linear cascade consists of nine Pratt and Whitney Pak B blades, which span a 95-deg turn. Trailing-edge splitter plates (tail boards) were attached to the trailing edges of the most outboard and inboard blades to aid the flow in negotiating the turn and to maintain the correct pressure gradient on the blades. The angles of the tail boards were adjusted so that at high chord Reynolds numbers the pressure distribution on the blades agreed with high-Reynolds-number (Euler) calculations.

The top wall of the cascade section and side walls of the straight section downstream of the cascade are made of clear Lexan or plate glass to allow optical access for laser-Doppler-velocimetry (LDV) measurements. Photographs of the cascade section are shown in Fig. 2.

The Pak B blades were cast in an acrylic polymer in a numerically machined aluminum mold. The chord dimension is 7.89 in. (20.05 cm). These are designed to span the full height of the cascade section less a 0.25-in. (0.64-cm) gap at each end. The blades have threaded inserts that are molded into the blade ends to accept mounting bolts. The mounting bolts pass through the top and bottom walls of the cascade section. Round spacer washers take up the gap between the blade ends and the top and bottom walls.

The center blade was molded with 40 0.0625-in. (1.6-mm)-diam pressure ports on the surface. The chordwise positions of the taps are shown on the drawing of the Pak B section profile in Fig. 3. A

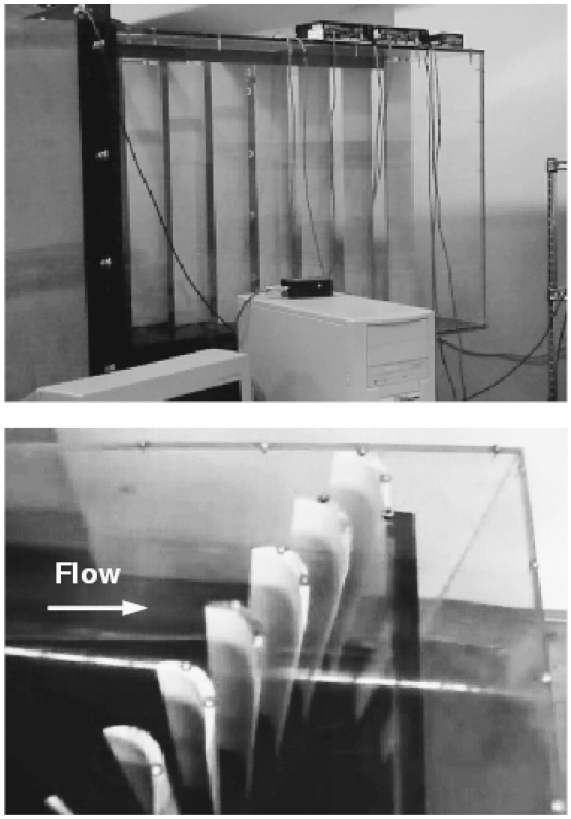

Fig. 2 Top and side-view photographs of Pak B blade cascade.

majority of the taps is on the suction side of the blade, with a special concentration in the region of $0.5 \le x/C \le 0.7$, where the flow is expected to separate at lower Reynolds numbers. The pressure taps are located at the midspan location of the blade and are distributed in the chordwise direction. A smaller number of taps were located at other spanwise positions and were only used early in the study to confirm the two-dimensionality of the blade-pressure distribution. The surface pressure is transmitted through 0.0625-in. (1.6-mm)-diam tubulations that are molded inside the blade and exit through the bottom end. These connected to a scanning pressure valve that multiplexed each pressure port to a single differential pressure transducer made by Validyne Corp. (Model DP103). The measurement uncertainty in the pressure coefficients is $\pm 1.9\%$.

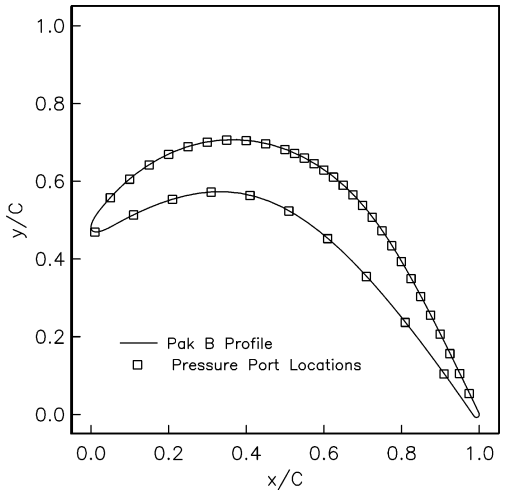

Fig. 3 Pak B section shape and locations of surface-pressure ports.

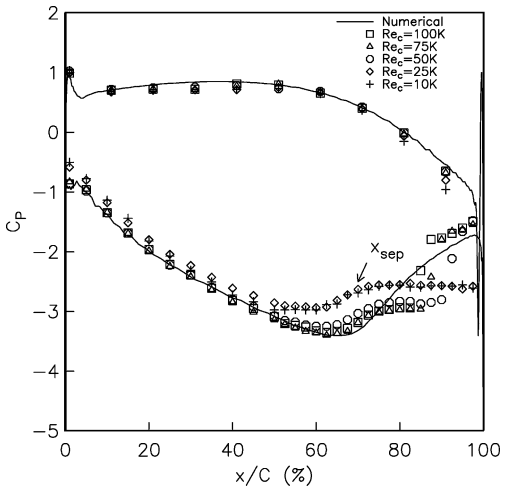

Fig. 4 Blade pressure coefficient distributions for different Reynolds numbers, for the lowest freestream turbulence level ($u'/U_\infty = 0.08\%$), and comparison to Euler simulation (Romeo, S., private communication, "Politehnica," Univ. of Timişoara, Romania, 2002).

III. Experimental Results

A. Baseline Conditions

The objectives of the baseline measurements were to document the effect of the chord Reynolds number and turbulence level on the locations of flow separation and reattachment on the suction side of the blade. This was documented through the surface-pressure coefficient $C_p = (P_s - P_\infty)/q$, where P_s is the blade surface pressure, $q = 1/2\rho U_\infty^2$, and U_∞ and P_∞ are measured in the straight section upstream of the cascade.

The C_p distribution on the blade for the Reynolds number range, $10^4 \leq Re_c \leq 10^5$, and the lowest freestream turbulence level of $u'/U_\infty = 0.08\%$, is shown in Fig. 4. Also shown is the computed pressure distribution based on an Euler (inviscid) code. The computations are equivalent to an infinite Reynolds number. Therefore they should indicate the distribution without flow separations. Comparing the measured distribution to the calculated distribution clearly indicates the region(s) of separation.

Defining the location of separation requires some judgment. In this paper we consistently mark it as the point of inflexion in the region of increasing C_p, near the trailing edge of the suction side of the blade. For the conditions in Fig. 4, this point occurs near $x/C \simeq 0.70$ as indicated.

The location of reattachment is easier to define. We mark it as the location where the C_p value jumps from the nearly constant values that are the hallmark of a separated region and begins to follow

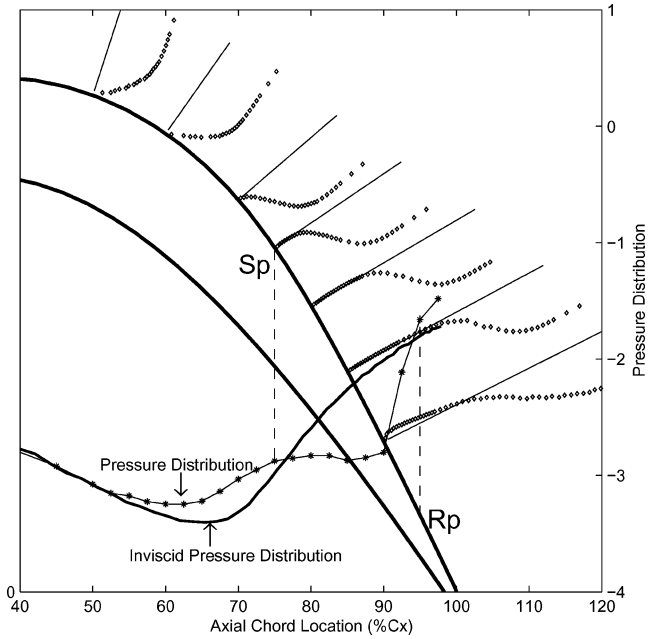

Fig. 5 Comparison between separation and reattachment locations based on surface-pressure distribution and mean velocity profiles obtained using LDV for lowest freestream turbulence level at $Re_c = 5 \times 10^4$. (Uncertainty in local mean velocity is ±0.56 to 95% confidence level of LDV.)

the inviscid distribution close to the trailing edge. At $Re_c = 10^5$, this occurs at $x/C \simeq 0.85$. For Re_c below 2.5×10^4, the flow never reattaches at this low-turbulence condition.

To gain further confidence in our ability to define the locations of the flow separation and reattachment based on the the surface-pressure distributions, Fig. 5 shows the corresponding mean velocity profiles obtained from LDV measurements. These measurements were obtained at $Re_c = 5 \times 10^4$. The corresponding measured (symbols) and inviscid (solid curve) pressure distributions are also presented in Fig. 5. Note that the development of an inflectional velocity profile occurs just downstream of the location of the minimum surface pressure. The vertical dashed lines show the reference locations on the blade where based on the pressure the flow separates (Sp) and reattaches (Rp). The agreement with the measured velocity profiles appears to be quite good.

The locations of the separation and reattachment for the low-disturbance condition are summarized in Fig. 6. The region between the two curves corresponds to a separation bubble that exists on the suction side of the blade. Note that the separation location is fairly insensitive to Re_c, whereas the reattachment location varies significantly. The effect of higher freestream turbulence levels is investigated next.

Turbulence generators were designed to give a range of higher freestream turbulence levels. Two were selected. The one labeled grid 3 corresponds to a perforated plate with 0.25-in. (6.3-mm)-diam holes, a mesh size of 0.313 in. (7.95 mm), and a solidity of 0.42. The grid was held in a frame that fit within the straight section, upstream of the Pak-B cascade. The position of the frame could be moved to place the grid at different streamwise distances from the cascade. This distance was referenced to the instrumented center blade.

The other turbulence generator, designated grid 0, was a mesh of 0.1875-in. (4.76-mm) diam cylinders. The mesh size (centerline spacing) in this case was 1.0 in. (2.54 cm). This was also held in a frame that fit in the section upstream of the cascade.

The turbulence intensity of each of the three velocity components was measured at different distances downstream of the two grids using a dual hot wire. The sensors were configured in an X arrangement to measure either (u, v) or (u, w) simultaneously. The results are shown in Figs. 7 and 8. These show the turbulence intensity u'/U_∞ and the local ratios u'/v' and u'/w'. These ratios are intended to show the degree of isotropy, which would be perfect

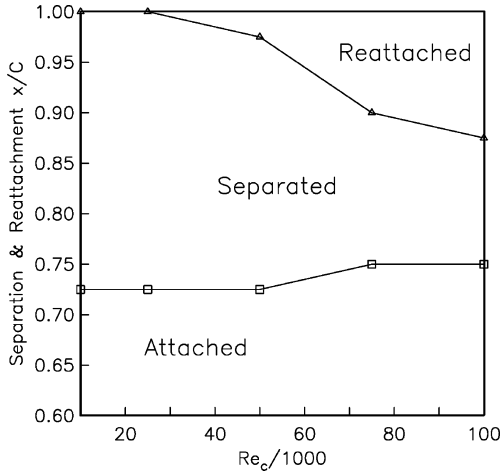

Fig. 6 Blade suction-side separation and reattachment locations as a function of Reynolds number for lowest freestream turbulence level ($u'/U_\infty = 0.08\%$).

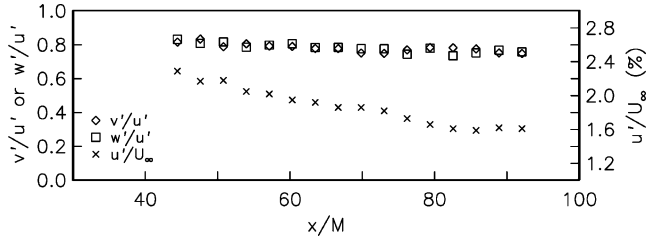

Fig. 7 Turbulence intensity (u'/U_∞) and degree of isotropy (v'/u' and w'/u') as a function of streamwise distance for grid 3.

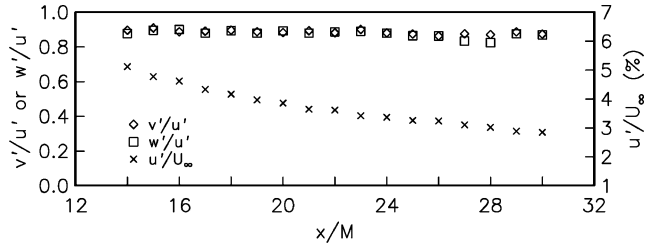

Fig. 8 Turbulence intensity (u'/U_∞) and degree of isotropy (v'/u' and w'/u') as a function of streamwise distance for grid 0.

if both were one. In reality, having $u'/v' \simeq u'/w'$ and ≥ 0.9 is considered quite satisfactory as an indication of isotropic nature of the turbulent scales.

With grid 3 (Fig. 7), the turbulence level varied from approximately 2.4 to 1.6%. The ratios of the fluctuating components were approximately 0.8 throughout the range of distances from the grid, suggesting a small deviation from isotropy between the fluctuating velocity components. The condition we chose to use for this grid occurred by placing the grid the farthest distance from the center blade. This gave a freestream turbulence level of $u'/U_\infty = 1.6\%$. Note that this turbulence level was 20 times larger than the freestream turbulence level without the grid.

With grid 0 (Fig. 8), the turbulence level varied from approximately 5.1 to 2.8%. The ratios of the fluctuating components had values of approximately 0.9 throughout the range of distances from the grid. This indicates a turbulence somewhat closer to a condition of isotropy than that which occurred with grid 3. The condition we chose to use for this grid occurred by again placing it the farthest distance from the center blade. This gave a freestream turbulence level of $u'/U_\infty = 2.85\%$. This turbulence level was 36 times larger than the freestream turbulence level without the grid, and 1.75 times that of grid 3.

The effect of the higher turbulence level of $u'/U_\infty = 1.6\%$ on the C_p distribution is shown in Fig. 9. These data are for the full

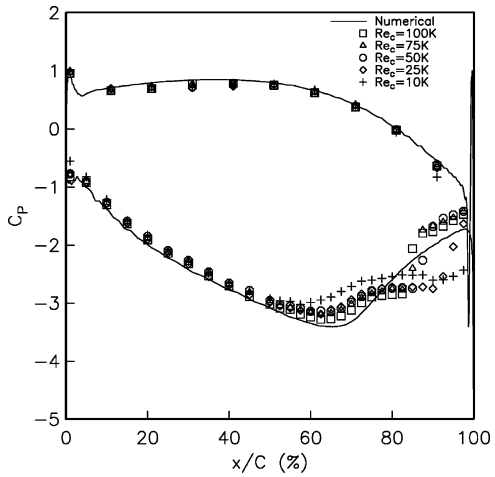

Fig. 9 Blade-pressure coefficient distributions for different Reynolds numbers, for the middle freestream turbulence level ($u'/U_\infty = 1.60\%$), and comparison to Euler simulation (Romeo, private communication).

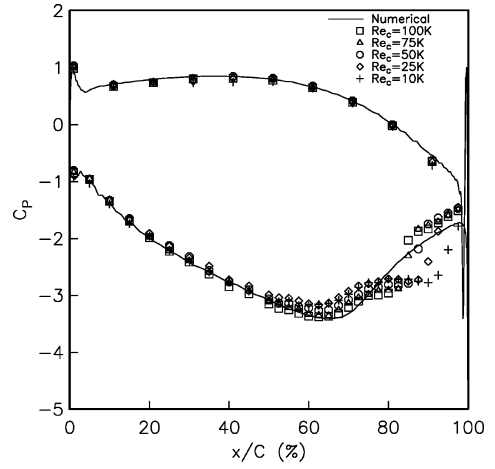

Fig. 10 Blade-pressure coefficient distributions for different Reynolds numbers, for the highest freestream turbulence level ($u'/U_\infty = 2.85\%$), and comparison to Euler simulation (Romeo, private communication).

range of Reynolds numbers, $10^4 \leq Re_c \leq 10^5$. Again the pressure distribution based on an Euler (inviscid) code is also presented. The C_p distributions indicate a relative insensitivity of the separation location to the higher freestream turbulence level. The separation location is still approximately at $x/C = 0.7$. However, compared to the low-turbulence condition in Fig. 4, and with the exception of $Re_c = 10^4$, the location for reattachment has moved upstream with the higher freestream turbulence level. This is perhaps most dramatic at $Re_c = 2.5 \times 10^4$, which did not reattach at the lower turbulence level.

The C_p distributions for the highest turbulence level of $u'/U_\infty = 2.85\%$ are shown in Fig. 10. This higher turbulence level had a minimal effect on the reattachment location compared to the previous case at $u'/U_\infty = 1.60\%$. However, aside from this separation region, the distributions collapse much better onto the Euler solution. In particular, near the leading edge on the pressure side of the blade we observe much better agreement at the high turbulence level. Comparing this region on the blade to the other cases in Figs. 4 and 9, we suspect that a small separation bubble exists just downstream of the leading edge on the pressure side. The highest turbulence levels in this case are enough to cause this to collapse. We plan to use LDV measurements to investigate this aspect further.

Based on the C_p distributions, the separation and reattachment locations on the suction side of the blade were compiled as in Fig. 6

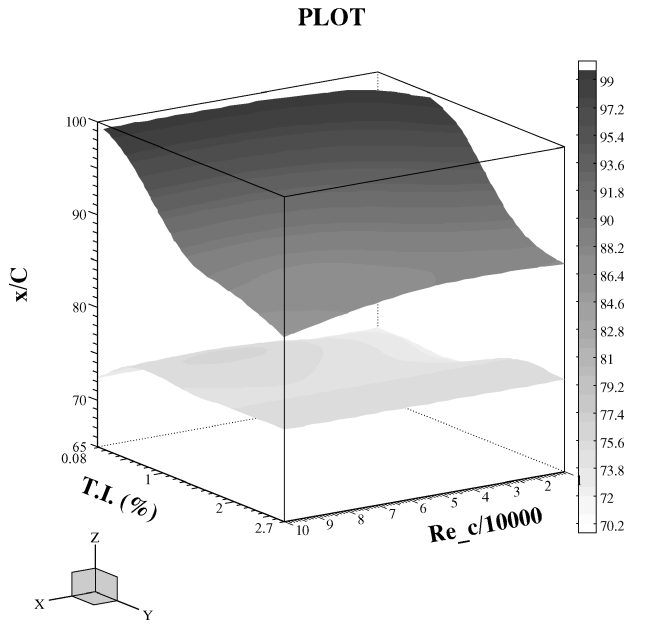

Fig. 11 Combined effect of chord Reynolds number and freestream turbulence level on the separation (bottom surface) and reattachment (top surface) locations on the suction side of the Pak B blade.

to include the effect of both Reynolds number and turbulence level. This is shown as a three-dimensional plot in Fig. 11. These results include the full range of Reynolds numbers from 10^4 to 10^5, for the three turbulence levels, 0.08, 1.60, and 2.85%.

The lower surface in the plot corresponds to the separation locations. In general, these tend to be relatively insensitive to the changing conditions, especially compared to the reattachment location, which corresponds to the upper surface. This is an important result. For most effective active flow control we want the actuator to be placed slightly upstream of the separation location. Because the separation location is relatively fixed for all of the conditions, only a single actuator, at one well-defined location, is required.

The upper surface in the plot corresponds to the reattachment locations. In general these are most sensitive to Reynolds number and somewhat sensitive to the turbulence level. For our conditions, at the highest turbulence level and Reynolds number, a separation bubble still remained on the pressure side if the blade.

B. Baseline Vortex Generators

Because streamwise vortex generators were found to be effective for separation control on cascade blades,[3,4] we investigated this passive approach in order to provide a basis for comparison to the active control with plasma actuators. The vortex generators consisted of brass shim material that was bent in a 90-deg angle. They were placed upstream of the separation line, at $x/C = 0.4$, along the span of the blade. The total height of the generators was approximately 1.3 times the local boundary-layer thickness. Two spanwise spacings were investigated: 0.5 and 1.0 in. (1.27 and 2.54 cm). The latter was comparable to the spacing used in Ref. 3. A photograph of the vortex generators on the center blade is shown in Fig. 12.

C_p distributions are presented for the 2.54-cm spaced vortex generators in Fig. 13 for Reynolds numbers from 10^4 to 10^5 at the lowest freestream turbulence condition (0.08%). Focusing on the suction side, the sawtooth variation at $x/C \simeq 0.4$ is caused by the vortex generators that partially obstruct the pressure taps at that location. Comparing the results to those in Fig. 4 (without vortex generators) indicates that they substantially reduced the extent of the separation region at all Reynolds numbers. For $Re_c \geq 7.5 \times 10^4$, the flow separation was eliminated completely, which is evident by the overlap of these C_p distributions with the Euler distribution.

Although vortex generators such as these tabs or dimples[3] are effective in controlling separation, they produce a drag penalty when not needed. The potential of the plasma actuators is that they can

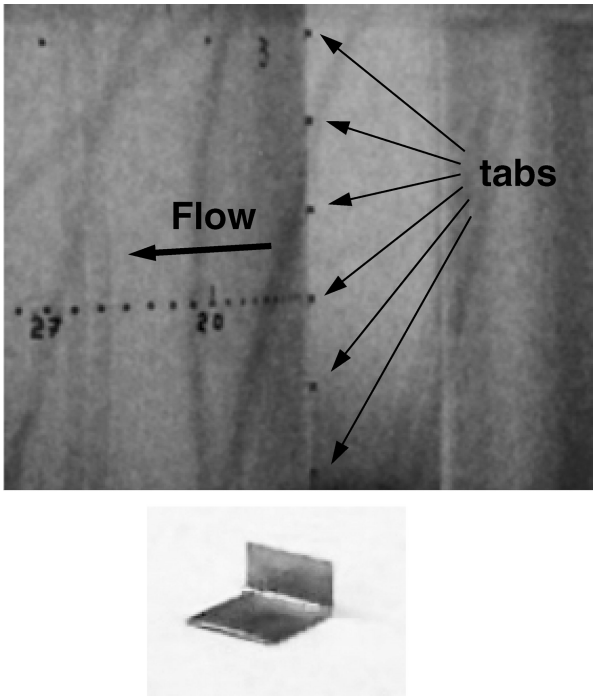

Fig. 12 Photograph of vortex generator "tabs" on center blade in cascade and an individual vortex generator. Spanwise spacing is 2.54 cm, and tab height is 1.6 mm.

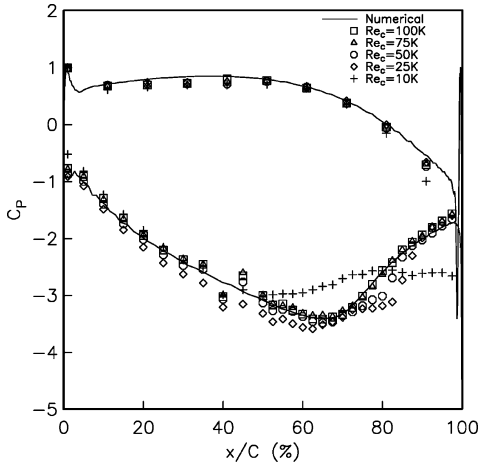

Fig. 13 Blade-pressure coefficient distributions with 1.0 in. spacing of vortex generators for different Reynolds numbers at the lowest freestream turbulence level ($u'/U_\infty = 0.08\%$) and comparison to Euler simulation (Romeo, private communication).

be made flush to the surface, and operated only when necessary, to eliminate any parasitic drag when not in use.

C. Plasma Actuators

The plasma actuators consist of two electrodes that are separated by a dielectric material. A high voltage ac input is supplied to the electrodes. When the ac amplitude is large enough, the air ionizes in the region of the largest electric potential. This is generally at the edge of the electrode, which is exposed to the air. The ionized air, in the presence of an electric field gradient, produces a body force on the bulk air.[13] The air near the electrodes is weakly ionized, and there is little or no heating of the air. In our applications, the power delivered to the electrodes is only approximately 20–40 W per linear foot of the actuator.

The body force per volume of plasma is a vector, given as

$$\boldsymbol{F}_B = \left[-\left(\epsilon_0 / \lambda_D^2\right)\phi\right]\boldsymbol{E} \tag{1}$$

where ϵ_0 is 8.854×10^{-12} F/m, and

$$\boldsymbol{E} = -\nabla\phi \tag{2}$$

The Debye length is the characteristic length for electrostatic shielding in a plasma. It varies with plasma density and temperature as

$$1/\lambda_D^2 = \left(e^2 n_0/\epsilon_0\right)(1/kT_i + 1/kT_e) \tag{3}$$

In one dimension, Eq. (1) reduces to

$$\boldsymbol{F}_B = (\epsilon_0/2)(\nabla|\boldsymbol{E}|^2) \tag{4}$$

which we have used in the past[5] to obtain an estimate of the body-force vector for use in the design of actuator electrode arrangements.

The body-force vector can be tailored through the design of the electrode arrangement, which controls the spatial electric field. Post[7] demonstrated arrangements that could produce wall jets or spanwise or streamwise vortices, when placed on the wall in a boundary layer. The body-force representation is also a convenient form to incorporate the effect of the actuators in Navier–Stokes simulations of the flowfield.[5] Such simulations are useful in designing and optimizing actuator arrangements.

Our first approach for controlling separation on the Pak B blades using the plasma actuators was to use a design that would produce a steady two-dimensional wall jet to energize the flow near the location of separation. This is illustrated in Fig. 14.

The actuator spanned most of the length of the center blade in the cascade. It consisted of a pair of electrodes separated by a dielectric layer. This sandwich arrangement was bonded to the blade surface. The electrodes consisted of 0.5-in. (1.27-cm)-wide, 0.001-in. (0.025-mm)-thick copper foil tape. The dielectric material consisted of three layers of 0.001-in.-thick Kapton film that were bonded together. The electrodes overlapped at one edge by approximately 0.040 in. (1 mm). The exact amount of overlap is not critical, but there needs to be some small amount to have a uniform plasma in the full spanwise direction.

The plasma forms starting at the overlapped edge of the electrode that is exposed to the air. This corresponds to the region of the largest electric field potential. The body force increases with the voltage amplitude in proportion to the volume of plasma (ionized air) and the strength of the electric field gradient. This electrode design produces a body force that draws ambient fluid toward the wall and then jets the fluid in the downstream direction (from right to left in Fig. 14).

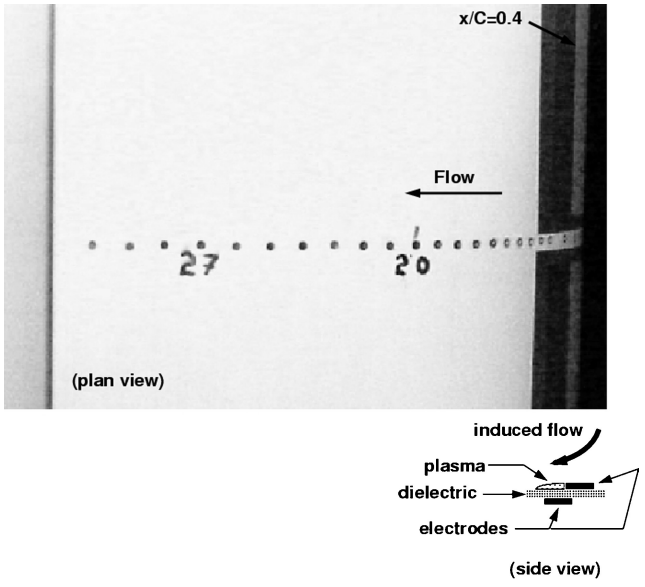

Fig. 14 Photograph of plasma actuator at the $x/C = 0.4$ location on blade with pressure ports and schematic of electrode arrangement and induced velocity direction.

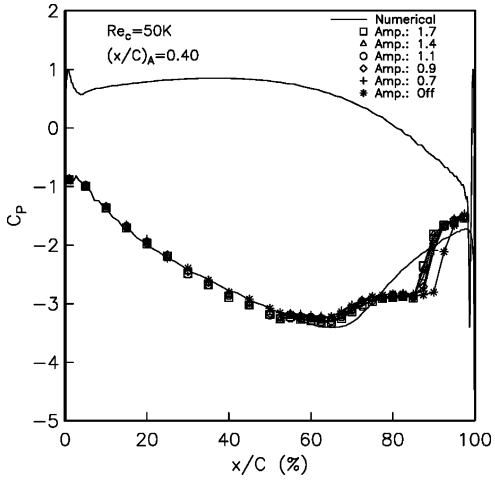

Fig. 15 Blade-pressure coefficient distributions with plasma actuator at $x/C = 0.4$ for different actuation levels at $Re_c = 5 \times 10^4$.

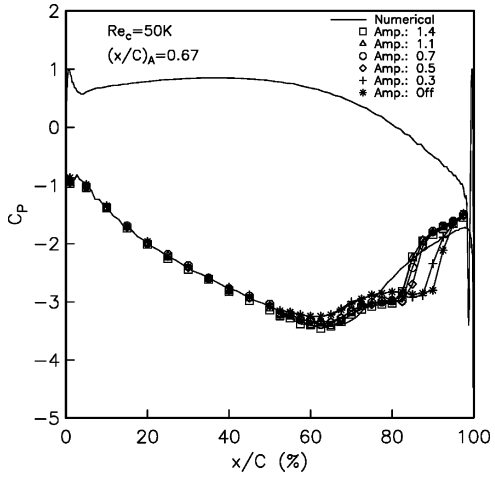

Fig. 16 Blade-pressure coefficient distributions with plasma actuator at $x/C = 0.675$ for different actuation levels at $Re_c = 5 \times 10^4$.

The ac voltage supplied to the electrodes was at a frequency of 5 kHz. This was selected primarily on electronic considerations. With regard to the flow, the effect can be considered to be steady, for example, a steady wall jet. We have the capability of producing unsteady effects at low frequencies (down to a fraction of a hertz if desired), but the results to follow were at steady conditions.

The ac voltage level needed to locally ionize the air, and control reattachment was investigated as part of this effort. This is mainly a function of the actuator design (electrode arrangement and dielectric properties). In our configuration the nominal voltage was 5 $kV_{p\text{-}p}$, and the power to the electrodes was approximately 20 W.

Two actuator locations of $x/C = 0.4$ and 0.675 were investigated. The actuator location is defined as the x/C position of the edge of the exposed electrode. All of the results to be presented were obtained at the lowest freestream turbulence level condition. In addition, all of the comparisons were made against the passive actuator-off condition to account for any small effects the surface application of the actuator had on the flow.

Figure 15 documents the blade-pressure coefficient distribution on the suction side for different actuator levels with the actuator at $x/C = 0.4$. This position is well upstream of the separation location, which, based on Fig. 6, occurs at $x/C \simeq 0.70$.

In Fig. 15, the star symbols indicate the C_p distribution with the actuator off. For this Re_c, the flow reattaches at $x/C \simeq 0.95$. Increasing the actuator amplitude moves the point of reattachment upstream. At the largest amplitude the point of reattachment is $x/C \simeq 0.90$.

One would expect that the actuator should be located closer to the point of separation to be most effective. Figure 16 therefore

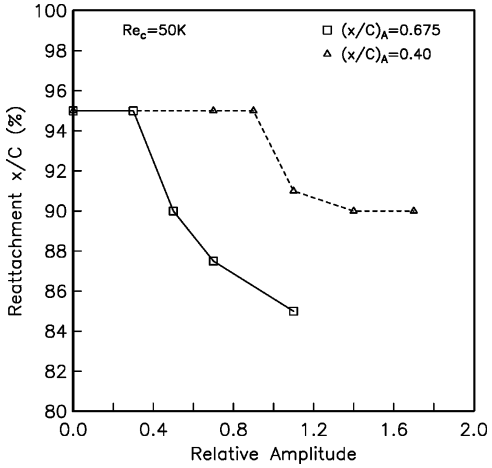

Fig. 17 Effect of plasma actuator amplitude on reattachment location for two actuator *x/C* positions ($Re_c = 5 \times 10^4$).

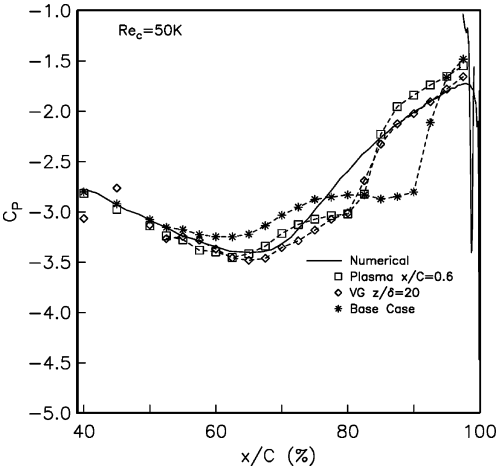

Fig. 18 Comparison of pressure coefficient distributions in the separation region for vortex generator tabs at two spacings and plasma actuator at $x/C = 0.675$ ($Re_c = 5 \times 10^4$).

documents the effect of placing the actuator at $x/C = 0.675$. Again the star symbols indicate the condition with the actuator off.

With the actuator located at the farther downstream position, we observe a much larger effect. There also appears to be a saturation effect of the amplitude on the point of reattachment. That is, there is a threshold amplitude above which the reattachment point is not changed appreciably.

These results are summarized in Fig. 17. This shows the reattachment location as a function of the actuator amplitude for the two x/C actuator locations at $Re_c = 5 \times 10^4$.

At this point it is relevant to compare the effect of separation control between the vortex generator tabs and the plasma actuators. This is done by cross-plotting the C_p distributions on the suction side of the blade in the region of separation. Here we consider only the best of the plasma actuator conditions ($x/C = 0.675$ and largest amplitude).

The comparison is presented in Fig. 18. Included are the base condition (without actuation) and the numerical inviscid distribution. We observe that the pressure distributions for the two actuator approaches are nearly identical. Both significantly reduce the separation region. However, the advantage of the plasma actuator design is that they can be turned off when not needed and when off, do not produce any parasitic drag.

IV. Summary

A linear cascade of Pak B blades was studied over a range of chord Reynolds numbers from 10^4 to 10^5 and a range of freestream turbulence levels from $u'/U_\infty = 0.08$ to 2.85%. Using an instrumented center blade, the flow was documented on the basis of the surface-pressure distribution. These revealed a separation region on the suction side of the blade that is consistent with the loss of efficiency in the low-pressure turbine stage at low Reynolds number found by Sharma.[2]

For the range of conditions studied, the separation location was nearly independent on the chord Reynolds number and freestream turbulence level. The nominal location was at $x/C = 0.7$. The location of reattachment was found to be strongly dependent on the chord Reynolds number and slightly dependent on the turbulence level. In all cases, some separation region existed. At the lower chord Reynolds numbers, $Re_c < 5 \times 10^4$, at all but the highest turbulence level the flow never reattached. Even at the highest Reynolds numbers and turbulence levels, a separation zone was always present on the suction side of the blade.

Plasma actuators for separation control were examined and contrasted to the performance of tab vortex generators. The x/C location and spanwise spacing of the tabs were consistent with the "dimples" used by Lake et al.[3] A single plasma actuator was examined. It was designed to produce a steady two-dimensional wall jet in the flow direction and thereby add momentum to the boundary layer. Two x/C locations of the plasma actuator were examined, 0.4 and 0.675. Actuators in both locations could affect the separation, although the actuator in the downstream position, closer to the separation location, was more effective.

Overall, we obtained performance from plasma actuators that was comparable to that of the vortex generators. Both were able to substantially reduce the separation distance. The advantage of the plasma actuator, however, is that they can be operated only when needed, and when not in use, produce no parasitic effects.

Acknowledgments

This work was supported by a grant from the NASA John H. Glenn Research Center, NCC3-775, and monitored by David Ashpis.

References

[1]Hourmouziadis, J., "Aerodynamic Design of Low Pressure Turbines," AGARD 167, 1989, pp. 8.1–8.40.

[2]Sharma, "Impact of Reynolds Number on LP Turbine Performance," NASA CP-1998-206958, 1998, pp. 65–70.

[3]Lake, J. P., King, P. I., and Rivir, R. B., "Reduction of Separation Losses on a Turbine Blade with Low Reynolds Number," AIAA Paper 99-0242, 1999.

[4]Bons, J., Sondergaard, R., and River, R., "Control of Low-Pressure Turbine Separation Using Vortex Generator Jets," AIAA Paper 99-0367, 1999.

[5]Orlov, D., Erturk, E., Post, M., and Corke, T., "DNS Modeling of Plasma Array Flow Actuators," *Bulletin of the American Physical Society Fluid Dynamics Division*, Vol. 46, No. 10, 2001, p. 217.

[6]Corke, T. C., and Matlis, E., "Phased Plasma Arrays for Unsteady Flow Control," AIAA Paper 2000-2323, 2000.

[7]Post, M. L., "Phased Plasma Actuators for Unsteady Flow Control," M.S. Thesis, Univ. of Notre Dame, Notre Dame, IN, 2001.

[8]Corke, T., Cavalieri, D., and Matlis, E., "Boundary Layer Instability on a Sharp Cone at Mach 3.5 with Controlled Input," *AIAA Journal*, Vol. 40, No. 5, 2002, pp. 1015–1018.

[9]Corke, T., Jumper, E., Post, M., Orlov, D., and McLaughlin, T., "Application of Weakly-Ionized Plasmas as Wing Flow-Control Devices," AIAA Paper 2002-0350, 2002.

[10]Post, M., and Corke, T., "Separation Control on High Angle of Attack Airfoil Using Plasma Actuators," *AIAA Journal*, Vol. 42, No. 11, 2004, pp. 2177–2184; also AIAA Paper 2003-1024, 2003.

[11]Hultgren, L., and Ashpis, D., "Demonstration of Separation Delay with Glow-Discharge Plasma," AIAA Paper 2003-1035, 2003.

[12]List, J., Byerley, A., McLaughlin, T., and VanDyken, R., "Using Plasma Actuator Flaps to Control Laminar Separation on Turbine Blades in a Linear Cascade," AIAA Paper 2003-1026, 2003.

[13]Enloe, L., McLaughlin, T., VanDyken, R., Kachner, K., Jumper, E., and Corke, T., "Mechanisms and Response of a Single Dielectric Barrier Plasma," AIAA Paper 2003-1021, 2003; also *AIAA Journal*, Vol. 42, No. 3, 2004, pp. 589–594.

H. Reed
Associate Editor